# The processing of compound radial frequency patterns

Gunnar Schmidtmann[a],[*], Frederick A.A. Kingdom[b], Gunter Loffler[c],[*]

[a] *Eye & Vision Sciences Research Group, School of Health Professions, University of Plymouth, Plymouth, Devon, England, United Kingdom*
[b] *McGill Vision Research, Department of Ophthalmology, McGill University, Montreal, Quebec, Canada*
[c] *Department of Vision Sciences, Glasgow Caledonian University, Glasgow, Scotland, United Kingdom*

## ARTICLE INFO

## ABSTRACT

Radial frequency (RF) patterns can be combined to construct complex shapes. Previous studies have suggested that such complex shapes may be encoded by multiple, narrowly-tuned RF shape channels. To test this hypothesis, thresholds were measured for detection and discrimination of various combinations of two RF components. Results show evidence of summation: sensitivity for the compounds was better than that for the components, with little effect of the components' relative phase. If both RF components are processed separately at the point of detection, they would combine by probability summation (PS), resulting in only a small increase in sensitivity for the compound compared to the components. Summation exceeding the prediction of PS suggests a form of additive summation (AS) by a common mechanism. Data were compared to predictions of winner-take-all, where only the strongest component contributes to detection, a single channel AS model, and multi-channel PS and AS models. The multi-channel PS and AS models were modelled under both Fixed and Matched Attention Window scenarios, the former assuming a single internal noise source for both components and compounds or different internal noise sources for components and compounds respectively. The winner-take-all and single channel models could be rejected. Of the remaining models, the best performing one was an AS model with a Fixed Attention Window, consistent with detection being mediated by channels that are efficiently combined and limited by a single source of noise for both components and compounds.

## 1. Introduction

Historically, subthreshold summation experiments have been successfully employed to demonstrate the existence of multiple spatial frequency (SF) tuned channels (Campbell & Robson, 1968; Graham & Nachmias, 1971; King-Smith & Kulikowski, 1975; Kulikowski & King-Smith, 1973; Sachs, Nachmias, & Robson, 1971) and to measure their orientation bandwidths (see Graham, 1989, for review). For example, Campbell and Robson (1968) and Graham and Nachmias (1971) measured contrast sensitivity for sinusoidal gratings with different SF (e.g. one grating with SF of 3c/deg and the other 9c/deg). The two gratings were then superimposed to form a compound pattern, and thresholds measured again. The rationale was that if both gratings were processed by a common broadband channel one would expect a substantial threshold reduction for the compound as their signals would combine additively. On the other hand, if the grating components were processed by separate channels, their signals would combine probabilistically resulting in only a marginal increase in sensitivity. The results from these experiments supported the existence of several narrowly tuned SF channels (Campbell & Robson, 1968; Graham & Nachmias, 1971).

Radial Frequency (RF) patterns, which are closed quasi-circular contours defined by sinusoidal modulations of their radius in polar coordinates, have frequently been used to investigate intermediate stages of shape processing (reviewed by Loffler, 2008 & Loffler, 2015; see also Schmidtmann & Fruend, 2019). Examples of RFs are shown along the horizontal and vertical axes of Fig. 1. In a typical RF experiment, subjects are presented with two patterns, one a circle, the other an RF with varying amplitude, and are required to detect the non-circular, RF shape. The minimum shape difference, measured as the amplitude of the sinusoidal modulation (see methods), at which observers can reliably discriminate between the circle and the RF pattern is the measured threshold. Several studies have suggested that different mechanisms are responsible for processing different RF shapes (Bell & Badcock, 2009; Bell, Badcock, Wilson, & Wilkinson, 2007; Bell, Wilkinson, Wilson, Loffler, & Badcock, 2009; Loffler, Wilson, & Wilkinson, 2003; Poirier & Wilson, 2006). For example, Bell et al. (2007) measured thresholds for combinations of RF patterns comprising low and high radial frequencies (e.g. RF3/RF24). They argued that if there are two independent channels, one for the low and one for the high RF, detection of one component should not be affected by the presence of the other, analogous to the rationale employed by the early studies on SF channels. Results supported this prediction. In a related experiment, Bell and Badcock (2009)

---
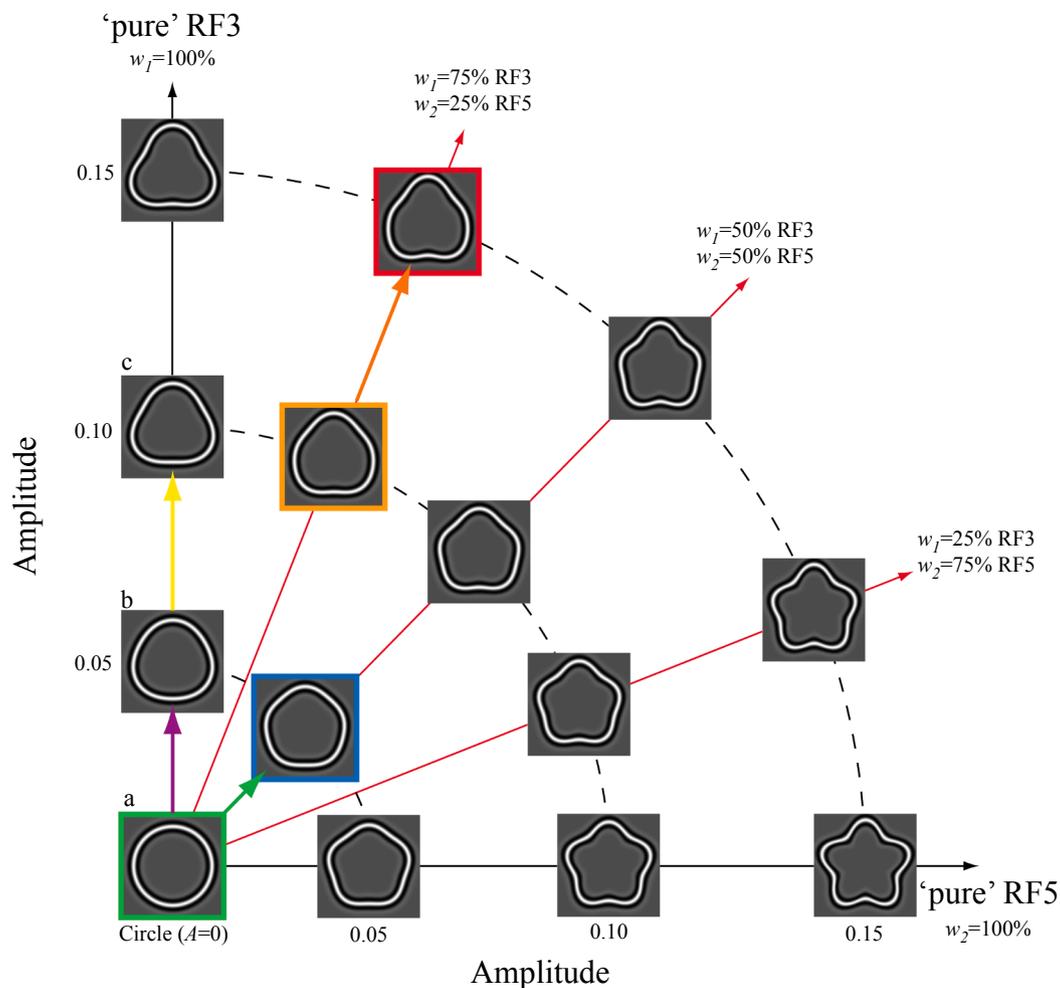
**Fig. 1.** Fraction of a theoretical shape space spanning between individual ('pure') RF3 and RF5 pattern (referred to as 'components' in this paper) and various combinations of them ('compounds'). In this shape space the circle in the green box represents the origin. The vertical and horizontal axes show respectively pure RF3 and RF5 patterns with increasing modulation amplitude (e.g. circle: $A = 0$; smoothed pentagon: RF5 with $A = 0.05$; five-pointed star: RF5 with $A = 0.15$). Combining two RF components with different weights ($w_{1/2}$) results in various compound 'morphs' as seen along the red arrows. The weights define the relative contribution of the two RF components to the compound pattern. In the experiments presented here, thresholds were determined for the pure RF components as well as for various weighted compounds. Weights of 100%/0% (pure RF3), 75%/25%, 50%/50%, 25%/75% and 0%/100% (pure RF5) were employed. (For interpretation of the references to color in this figure legend, the reader is referred to the web version of this article.)

applied a subthreshold summation paradigm to investigate the existence and nature of individual RF channels. They measured thresholds for isolated RF patterns and compared them to thresholds for compound RF patterns in which a second component, at half its threshold amplitude, was added. They argued that if both components were processed by a common channel, the signal from one RF component should be increased by the presence of the other component and overall thresholds should decrease even if the second component itself is presented at subthreshold levels. On the other hand, if the two components were processed by independent RF channels no such threshold reduction should occur. The results for low RFs ($\leq 10$) supported the latter prediction of independent RF channels. All these and other results (Bell et al., 2009) were taken as evidence for multiple RF channels.

Dickinson, Bell and Badcock (2013) explored RF pattern detection and identification at threshold. Their rational was that if subjects were able to identify different RF shapes at their respective detection threshold it would imply that the shapes were processed by discreet detectors/channels. Their results supported this notion but also showed a dependence on the amount of visible shape, e.g. if just a single cycle was presented identification at threshold was not possible. Based on these results, and as an alternative to shape decomposition into an RF base set, Dickinson et al. (2013) suggested that the periodicity of curvature

maxima (convexities) is the crucial feature that underpins RF detection. Dickinson et al. (2013) proposed that the cue that distinguishes the patterns with differing radial frequencies is the angle subtended between adjacent points of maximum curvature at the pattern centre. More recently, and in line with Dickinson, et al. (2013), Dickinson, Haley, Bowden, and Badcock (2018) demonstrated that RF3 patterns and similar patterns but with the same overall triangular-like shape, were very hard to discriminate. Given these findings, Dickinson et al. (2013, 2018) argue against a shape decomposition into discrete RF channels.

The main aim of this study was to probe how signals from two RF components are integrated when presented on a compound shape (see Fig. 1). We aim to determine if signals from the two components remain independent or if they are combined, and if they are combined, which process best describes the combination (see Fig. 2A vs. B, C). To do so, we measured detection (discrimination against circle) and discrimination (discrimination against pedestal amplitude)[1] sensitivity for a range

---

[1] Most of the previous studies were concerned with observer ability to discriminate an RF shape from a circle. This will subsequently be referred to as an RF detection task, to contrast it from RF discrimination, where observers have to discriminate two RFs: one with a pedestal amplitude and the other with an incremented amplitude.
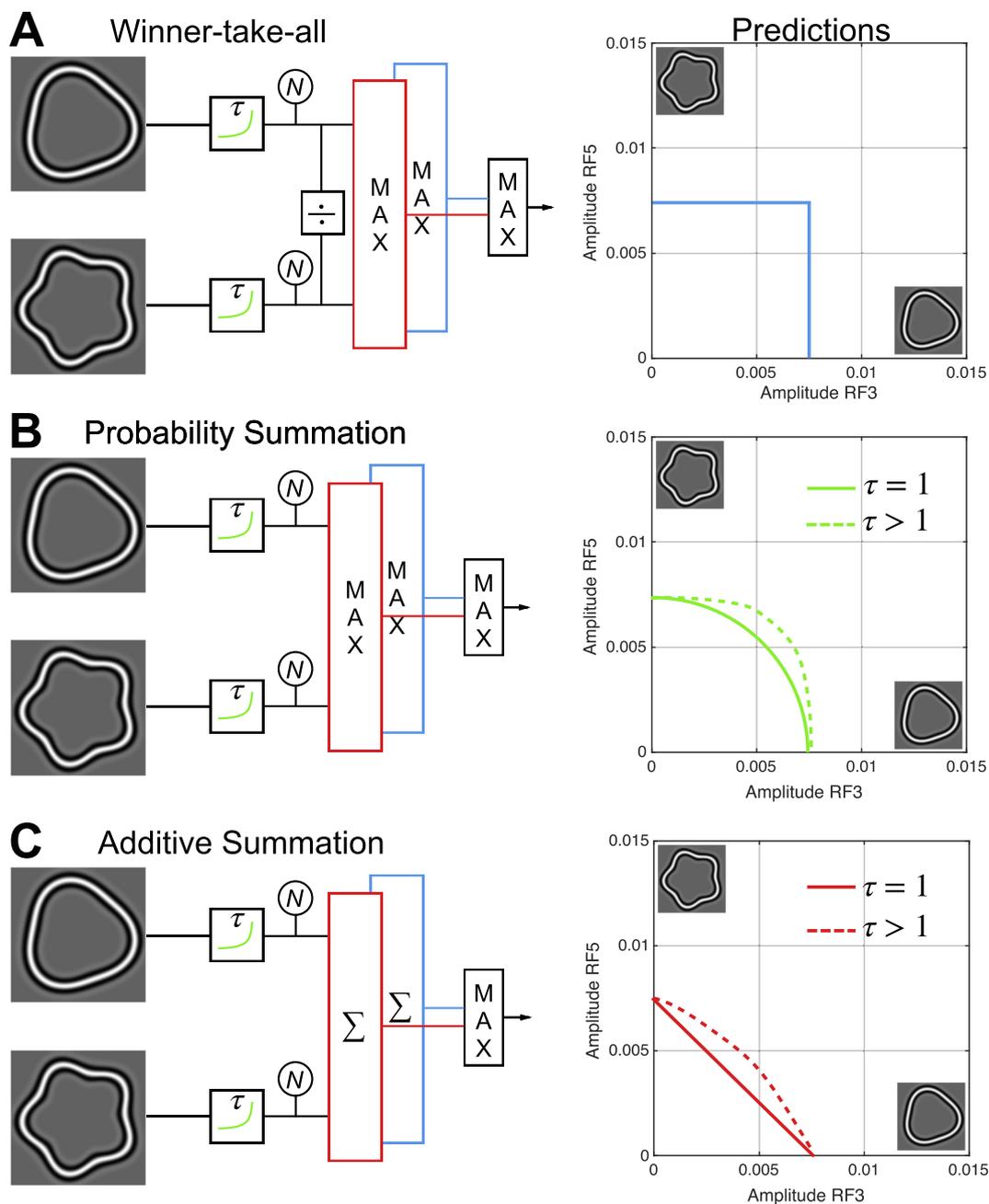
**Fig. 2.** Classes of summation scenarios considered within a signal detection theory framework (left column) and their corresponding predictions (summation plot in right column). In all 3 scenarios, the two components (shown by the grey-scale RF shapes) elicit a signal in a hypothetical shape channel. The signal within that channel depends on the amplitude of the component and is subject to a non-linear transducer ($\tau$ is the exponent of the transducer function) and an internal noise source ($N$). In the experiments, observers were shown two shapes in separate intervals and had to decide which was less circular (two-alternatives/intervals forced-choice paradigm). Each interval (e.g. circle vs RF compound with specific amplitude) will result in different signals and the two intervals are symbolized by the red and light blue rectangular boxes. MAX refers to a decision rule where the stronger signal is selected. Note that there are two MAX rules in some of the scenarios: in the case of probability summation, the stronger of the signals from the two channels in each interval is first selected and then the interval with the stronger signal determines the decision. The predictions on the right show the amplitudes of each component ($x$ and $y$ axis) for compounds at threshold (summation plots). (A) In the winner-take-all scenario only the strongest component contributes, the other is ignored or suppressed ($\div$). This results in predictions (right) for compound shapes that are determined by only one of the components. (B) In probability summation, each of the component channels contributes and the channel is selected that yields the stronger signal. Performance for the compound stimulus is better than that for the components because it allows two chances on which to base a decision. The predicted summation plots are consequently convexly curved and the amplitudes of each component when the compound is at threshold are lower than the thresholds for each component alone. (C) In additive summation (AS) the signals from the two component channels are summed and the summed signals compared between intervals, with the stronger signal selected. With AS the predicted thresholds are lower than PS. In the special case of linear transducers ($\tau = 1$), AS predictions fall on straight lines. In all scenarios, equal thresholds are assumed for the two components presented in isolation ($A = 0.0075$). (For interpretation of the references to color in this figure legend, the reader is referred to the web version of this article.)

of compounds. The compound shapes comprised various weighted combinations of two RF components (RF3/RF5; RF3/RF8; RF4/RF7).

## 1.1. Summation models

It may be helpful at the outset to outline the general predictions of the summation models we will entertain, each of which describes how component sensitivities are combined to derive predictions for compound performance. It is widely agreed that Signal Detection Theory provides a solid framework for describing decision-making processes in psychophysical experiments (Green & Swets, 1988; Laming, 2013; Meese & Summers, 2012; Nachmias, 1981; Tyler & Chen, 2000), and especially for experiments on signal summation (Meese & Baker, 2011; Schmidtmann, Jennings, Bell, & Kingdom, 2015b; Baldwin, Schmidtmann, Kingdom, & Hess, 2016). Hence, the data in this study are analyzed with models of summation based on Signal Detection Theory (Kingdom, Baldwin, & Schmidtmann, 2015).

Fig. 2 illustrates three possible model scenarios and their predictions. We distinguish between the rule for how the two signals from the two components of each compound shape in each trial are combined – the signal combination rule – and the rule for deciding which of the two sequentially presented compound shapes (forced-choice alternatives) – the decision rule. In all three models the latter, decision rule is a MAX rule, meaning that the observer chooses the alternative with the largest signal. This is represented by the rightmost MAX (black box) in the left panels of the figure. The three models differ in the signal combination rule, as symbolized in the red (first interval) and blue (second interval) rectangular boxes.

The model predictions are given in summation plots. These plots show the amplitude thresholds of the two components when they are presented in isolation (intersection of summation curve with the *x* and *y*-axis). Sensitivity for any compound (various weighted sums of the two components) is given by a point within the first quadrant as the amplitude of each component when the compound is at its threshold. When only one component is contributing, thresholds for various compound conditions would fall along straight horizontal and vertical lines: the compound is detectable if one of the component amplitudes is at its individual threshold.

This is the first model in Fig. 2A where only the strongest component contributes to detection, the other(s) being ignored or suppressed ($\div$). We refer to this as the "winner-take-all" model, termed "decision separability" by Macmillan & Creelman (2005). The other two models show cases where performance for compounds is better than that for the components. With probability summation, or PS, shown in Fig. 2B, a maximum (MAX) signal combination rule is applied: for each alternative the component with the biggest signal is selected. Thus, PS performance predicts higher sensitivity (lower thresholds) for the compound condition than for the components alone because there are two chances for a component signal to contribute to detection. The additive summation, or AS model in Fig. 2C, describes a scenario where the signals from the two components are summed within each interval/alternative. For all but the extreme parts of the summation square, where the compound comprises only one component, AS predicts lower thresholds than PS[2]. The precise shape of the summation curves for AS and PS depends on the transducers of the component channels ($\tau$, Eq. 2). While the summation curve for PS will always be convex, the shape for AS, and the degree of curvature for PS, depends on the exponents on the transducers of the component channels: for AS the shape is straight if the transducers are 1 and convex for values > 1, as shown by the dashed lines in Fig. 2B and C. A special case of AS is a Single Channel model, which assumes a single noise source.

The other aspect of summation to consider, which is not presented in Fig. 2, concerns how an observer attends to information from

different channels. For this, we contrast a Matched Attention Window (Kingdom et al., 2015) with a Fixed Attention Window (FAW, Tyler & Chen, 2000) scenario. The difference between the two lies in the number of channels that an observer monitors, which determines the amount of internal noise limiting performance. The Matched Attention Window (MAW) scenario assumes that the components are at least initially processed in separate channels and that the observer attends to only the channels that are known in advance to contain a signal; the other channels, together with their sources of noise, are ignored. Under the Fixed Attention Window scenario on the other hand both component channels are always monitored irrespective of whether or not they contain a signal, involving the obligatory pooling of the noise from both channels. As a consequence, when only one component is present the Matched Attention Window is the more efficient of the two scenarios, because there is only one source of noise limiting performance. It is important to bear in mind that both Matched and Fixed Attention Window scenarios are possible under PS and AS. Under AS, the Matched Attention Window scenario implies that the two components are initially processed by separate channels each with their own source of noise, prior to being additively combined by a single detection mechanism. With the Fixed Attention Window scenario under AS on the other hand, the signals from all monitored channel, together with their associated noises, are additively summed. We have also tested model scenarios where the exponent of the transducers of the component channels are fixed ($\tau_A = \tau_B$). In summary, we have tested nine different models: (1) AS FAW, (2) PS FAW, (3) AS MAW, (4) PS MAW, (5) AS FAW ($\tau_A = \tau_B$), (6) PS FAW ($\tau_A = \tau_B$), (7) AS MAW ($\tau_A = \tau_B$), (8) PS MAW ($\tau_A = \tau_B$), and (9) Single Channel. Each of the nine models was applied to individual data and not to averaged data. The model code and model simulations, including summation squares can be found at http://www.gunnar-schmidtmann.com/stimuli-software/#CompoundRF.

## 2. Methods

### 2.1. Subjects

Three observers participated in this study. Two of the participants were naïve as to the purpose of the experiment. All subjects had normal or corrected-to-normal visual acuity. Informed, written consent was obtained from each observer, and the study was approved by the Glasgow Caledonian University Ethics Committee. All experiments were conducted in accordance with the Declaration of Helsinki. Observations were made under binocular viewing conditions. No feedback was provided during practice or data collection.
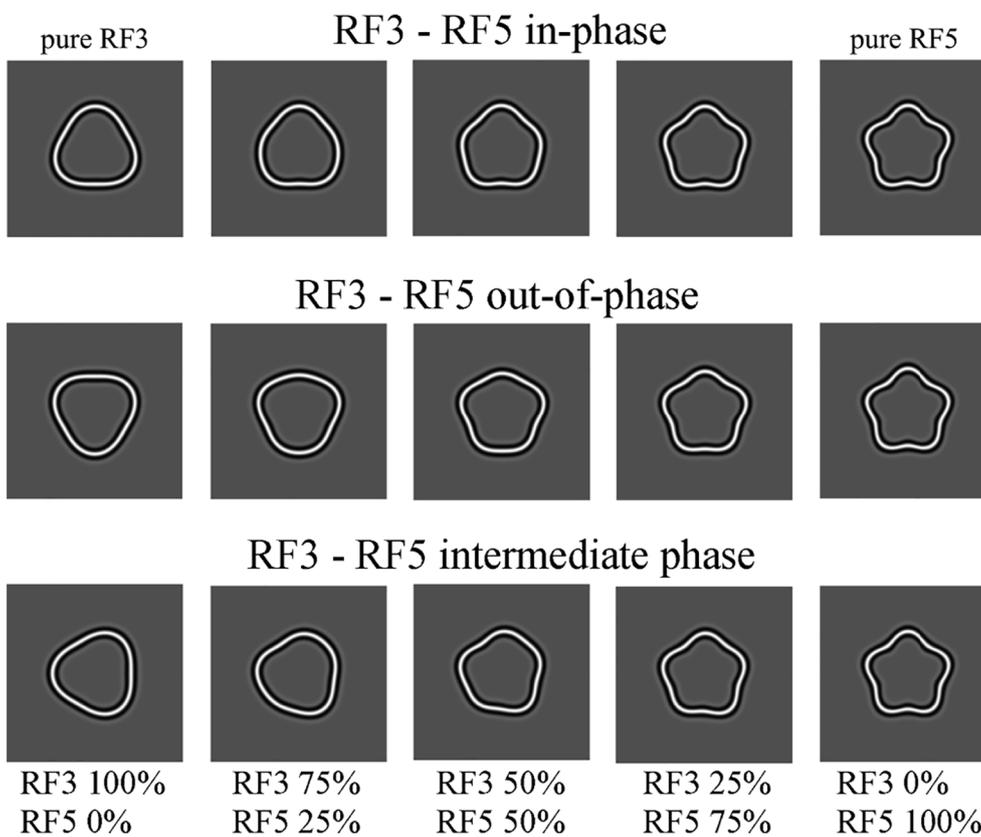
### 2.2. Apparatus

Stimuli were generated using Matlab 7.7 (Mathworks). The shapes were presented on a gamma-corrected LaCie "electron22blueII" monitor ($1024 \times 768$) with a frame rate of 85 Hz under the control of a Macintosh G4 computer. Monitor linearization was achieved by adjusting its color look-up table, resulting in 150 approximately equally spaced gray levels. The pattern luminance was on average 65 cd/m². Observers viewed the stimuli using a chin and forehead rest to guarantee a constant viewing distance of 120 cm. At this distance the size of 1 pixel was 0.018 deg. To minimize reference cues, a white cardboard mask with a circular aperture of 12 deg was placed in front of the monitor. Experiments were carried out under dim room illumination. Routines from the Psychophysics Toolbox were used to present the stimuli (Brainard, 1997).

### 2.3. Stimuli

The stimuli used in this study were weighted combinations of radial frequency (RF) patterns (Wilkinson et al., 1998), a class of closed

---

[2] Note that this is not shown in Fig. 2.

## RF3 - RF5 in-phase

pure RF3                                              pure RF5

## RF3 - RF5 out-of-phase

## RF3 - RF5 intermediate phase

RF3 100%    RF3 75%    RF3 50%    RF3 25%    RF3 0%
RF5 0%      RF5 25%    RF5 50%    RF5 75%    RF5 100%

**Fig. 3.** Example stimuli and phase-dependence. The rows show compound shapes formed by adding an RF3 and an RF5 pattern, where the two RF components are in-phase (top row), out-of-phase (mid row) and intermediate phase (bottom row). Columns are for five different combination weights. The left hand column shows pure RF3, the right hand column pure RF5 and the other columns show compounds. For the shape combinations used in this study, the in-phase and out-of-phase conditions result in symmetrical compound shapes, whereas the intermediate phase condition leads to asymmetrical compounds.

contour with varying shapes. An RF compound contour was defined as:

$$r(\theta) = r_{mean}\left[1 + w_1 \cdot A \cdot sin(\omega_1 \cdot \theta + \varphi_2) + w_2 \cdot A \cdot sin(\omega_2 \cdot \theta + \varphi_2)\right] \qquad (1)$$

where $r$ (radius) and $\theta$ refer to the polar coordinates of the contour and $r_{mean}$ is the radius of the modulated circle and determines the overall size of the pattern. It was set to 0.5 deg. $A$ defines the modulation amplitude, $\omega_1$, $\omega_2$ the radial frequencies and $\varphi_1$, $\varphi_2$ the phases (orientations) for each RF component, respectively. The variables $w_1$ and $w_2$ refer to the relative weights of the two RF components in percent. They were set so that $w_2 = 1-w_1$. Weights ($w_1/w_2$) (expressed in percent) of 100%/0%, 75%/25%, 50%/50%, 25%/75% and 0%/100% were used. The shapes with a weight relationship of 100%/0% and 0%/100% will be referred to as 'pure' RF patterns, as they contain only information from one RF component. Compound shapes were weighted combinations of the following component configurations: RF3/RF5, RF3/RF8 and RF4/RF7. The appearance of the resulting compound shape depends on the component frequencies, their amplitudes as well as their phase relationship. The phase relationship was either in-phase (a peak of each component aligned) or out-of-phase for combinations between an RF3 and an RF5 (a peak aligned with a trough). Additionally, an intermediate phase was used, defined as the point where the concave contour minimum, or trough of the higher RF component (RF5, 7 & 8) coincides with the point of inflection, or zero-crossing of the lower (RF3 & RF4) component (Fig. 3).

Pure RF patterns are symmetrical shapes, where the frequency, i.e. number of cycles determines the number of symmetry axes. For instance, an RF3 has three axes of symmetry and an RF5 has five. Combining different RF components in-phase and out-of-phase results in compound shapes with only one axis of bilateral symmetry, whereas combining the RF components with intermediate phases leads to asymmetrical shapes (see Fig. 3 for example stimuli with different phase relationships).

Consistent with previous studies the cross-sectional luminance profile of the stimuli was defined by a fourth derivative of a Gaussian

(D4) (Wilkinson et al., 1998) with a peak spatial frequency of 8 c/deg.

### 2.4. Procedure

The method of constant stimuli was employed using a temporal two-interval forced choice task. The monitor was initially set to a mid grey luminance level. The subject started the experiment by pressing a key on a standard computer keyboard. Each trial contained a reference and a target stimulus. After 300 ms the first stimulus was presented for 160 ms, followed by a mid grey screen for 300 ms (inter-stimulus interval), after which the second stimulus was presented for 160 ms. The observer's task was to indicate which of the two successively presented stimuli was the target, which was always the contour with the higher modulation amplitude (less circular). In the first experiment (RF detection) the target was the non-circular shape (green vs. blue in Fig. 1) which was always paired with a perfect circle as reference. In the second experiment (RF discrimination) the target was the more modulated shape (orange vs. red in Fig. 1). In the latter case the modulation amplitude $A$ of the reference shape was set to 0.05, which corresponds to approximately 10x detection threshold of an RF shape against a circle. The two patterns were always presented in random order and with random overall orientations. Different relative weights ($w_1$, $w_2$) and phase relationships ($\varphi_1$, $\varphi_2$) between the two components were run in separate blocks. Thresholds were defined as the minimum amplitude ($A$; Eq. (1)) required for reliable detection/discrimination. These compound amplitudes ($A$) were then converted into the respective component amplitudes at threshold by multiplication: $A \cdot w_1$ or $A \cdot w_2$.

The stimuli were presented at a random position within 0.124 deg from the centre of the screen. Each experimental condition was tested within separate blocks (e.g. RF3/RF5 in-phase). In each block, six different stimulus amplitudes were presented 30 times each, resulting in a total number of 180 trials per threshold estimate. Subjects completed three repetitions of each experimental condition. The data of each run

were fitted with a Quick psychometric function using a customized maximum- likelihood procedure based on binomial proportions, and MatLab's *fminsearch* function. Thresholds were defined as the point on the function where subjects made 75% correct responses.

### 2.5. Summation modeling

Apart from winner-take-all summation, the two possible scenarios for the processing of compound RF shapes are PS and AS. According to PS if the two RF components (*A* and *B*) are processed independently by separate narrowly-tuned shape channels, one would expect only a slight reduction in thresholds (improvement in sensitivity) for the RF compound compared to the components. On the other hand, according to AS, if the components are initially processed in separate shape channels but their signals are then added before a decision is made, one would expect a greater reduction in thresholds as the information from both RF components is used more efficiently.

Below we summarize the equations for PS and AS for the general case where stimulus strength of the two components can be unequal/different. Unequal sensitivities for the two components making up a compound is the typical scenario in the experiments presented below but the predictions differ from those illustrated in Fig. 2 where equal sensitivities were chosen for clarity. In order to derive the summation predictions, one has to make an assumption about first the number of channels that are activated by the stimulus and second the number of channels monitored by the observer. As discussed earlier, the analysis here considers two scenarios: Matched Attention Window (Kingdom et al., 2015) and Fixed Attention Window (Tyler & Chen, 2000). The difference between the two lies in the number of channels that an observer monitors (*Q*, see below*)*. Assuming that the two components are being processed in separate channels, there are two channels that can carry a signal. The observer can attend to one, the other or both. The Matched Attention Window scenario assumes that the observer can match their attention to the experimental condition and only attends to those channels that contain a signal. Under this scenario *Q*, the number of channels monitored, is the same as *n*, the number of channels carrying signals. Thus, when components are tested, *Q* and *n* both equal 1, while for the compound *Q* and *n* both equal 2. Given that the component and compound conditions were tested in separate blocks, we consider this a plausible scenario. Observers were, however, not informed whether in an individual block they were tested on a component or a compound. It is therefore also conceivable that they always monitored two channels - this is the Fixed Attention Window scenario. In this case, *Q* would be 2 for both components and compound conditions and *n* = 1 for the component and *n* = 2 for the compound. Hence, we modeled PS and AS under both scenarios.

### 2.6. Additive summation

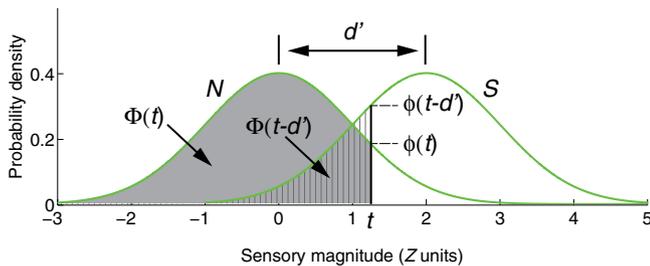Signal detection theory considers the internal strength of a signal as



**Fig. 4.** Parameters for calculating AS and PS. *N* = noise distribution, *S* = signal distribution, *d′* = separation between *S* and *N* distributions. *t* is a sample sensory magnitude. $\Phi(t)$ and $\Phi(t\text{-}d')$ are the areas under the *N* and *S* distributions to the left of *t*. $\phi(t)$ and $\phi(t\text{-}d')$, are the heights of the *N* and *S* distributions at *t*. Based on Figure 6.5 in Kingdom & Prins (2016).

the distance between two distributions: internal noise only and signal plus noise (see Fig. 4). This is expressed in units of standard deviations and referred to as *d′*. According to Kingdom et al. (2015), *d′ for* AS for stimulus components of unequal strength (i.e. different amplitudes for each of the two components making up the compound in our experiments) is given by:

$$d' = \frac{1}{\sqrt{Q}} \sum_{i=1}^{n} (g_i S_i)^{\tau_i} \tag{2a}$$

where $S_i$, $g_i$ and $\tau_i$ refer to the stimulus strength, gain and transducer exponent of the $i_{th}$ stimulus component respectively. *Q* and *n* are the number of monitored channels and the number of stimulus components respectively. In essence, this is calculating *d′* as the sum of the signals from each channel divided by the square root of the number of monitored channels. In the model simulations below, the stimulus strengths $S_i$ correspond to the component amplitudes; gains and transducers for each channel, $g_i$ and $\tau_i$, are free parameters set to best fit the data. The following equation is then used to calculate percent correct responses for a given stimulus strength and corresponding *d′* as (Kingdom & Prins, 2016; Fig. 4):

$$Pc = \int_{-\infty}^{\infty} \phi(t - d')\Phi(t)^{M-1}dt \tag{2b}$$

In these equations $\phi(t)$ and $\phi(t\text{-}d')$ refer to the heights of the signal (*S*) and noise (*N*) distributions at a sample point *t* and $\Phi(t)$ and $\Phi(t\text{-}d')$ refer to the areas under the *S* and *N* distributions to the left of *t*, as illustrated in Fig. 4. *M* indicates the number of alternatives in the forced-choice task (in all experiments here *M* = 2). The detailed mathematical derivations of the equations can be found in Kingdom et al. (2015) and Kingdom & Prins (2016). For the Matched Attention Window scenario, one simply sets *Q* equal to *n*; i.e. for the component *Q* = *n* = 1 and for the compound *Q* = *n* = 2. For the Fixed Attention Window scenario, *Q* = 2 and *n* = 1 for the components and *Q* = 2 and *n* = 2 for the compound. Note that if only the compound conditions were considered the two scenarios would make the same predictions, because *Q* = *n* = 2 in both cases. The equations for additive summation are implemented by the function PAL_SDT_AS_uneqSLtoPC in the Palamedes Toolbox (Prins & Kingdom, 2018)

### 2.7. Additive summation single channel

The Single Channel AS model assumes a single source of noise. The number of monitored channels is *Q* = *1*. This model has just two instead of four free parameters (*g* and *τ*).

$$d' = \sum_{i=1}^{n} (g S_i)^{\tau} \tag{2c}$$

### 2.8. Probability summation

Kingdom et al. (2015) showed that PS under SDT for stimuli of unequal strength under the Fixed Attention Window scenario with a 2AFC task is given by:

$$Pc = \sum_{i=1}^{n} \left[ \int_{-\infty}^{\infty} \phi(t - d'_i)\Phi(t)^{QM-n} \prod_{j=1, j\neq i}^{n} \Phi(t - d'_j)dt \right]$$
$$+ (Q - n) \int_{-\infty}^{\infty} \phi(t)\Phi(t)^{QM-n-1} \prod_{j=1}^{n} \Phi(t - d'_j)dt \tag{3a}$$

The first part of Eq. (3a), computes the probability that the *i-th* signal component will be greater than all noise components (total *QM-n*) and all other signal components (total *n-1*). These other signal components are designated as *j*, hence *j* refers to all signal components except the *i-th* signal component.

Analogous to AS, signal strength *d′* is calculated as:

$$d^{'} = (g_i S_i)^{\tau_i} \tag{3b}$$

Setting $Q$ equal to $n$ for Matched Attention Window scenario, gives:

$$Pc = \sum_{i=1}^{n} \left[ \int_{-\infty}^{\infty} \phi(t - d^{'}_i) \Phi(t)^{QM-n} \prod_{j=1, j\neq i}^{n} \Phi(t - d^{'}_j) dt \right] \tag{4}$$

### 2.9. Pedestal condition (Discrimination Experiment)

For the conditions containing a pedestal of amplitude 0.05 (discrimination experiment), we have modelled the data using the same model as for the zero pedestal conditions, i.e. fitting the multiple psychometric functions with the same free parameters of $g$ and $\tau$. We tried to fit the pedestal = 0.05 conditions with a model in which $d' = [g (S + \Delta S)]^{\tau} - (gS)^{\tau}$, where $S$ is the pedestal amplitude and $\Delta S$ the amplitude increment, but the minimization procedure we employed failed to converge on estimates of $g$ and $\tau$. We assume that the reason for this is because the above equation is not a good model for amplitude discrimination in RF patterns. In order to model the pedestal data (discrimination experiment), we have also tested various versions of alternative models, such as the Legge & Foley (1980) model that has been widely employed to model contrast discrimination data. However, in all cases we were unable to find a model which converged on consistent estimates of its free parameters, a problem often encountered in modeling psychophysical data when there are many free parameters to estimate. We are therefore making the assumption that treating the pedestal = 0.05 conditions as equivalent to the pedestal = 0 conditions does not have an adverse effect on our conclusions concerning the summation properties of RF patterns with two component frequencies.

### 3. Results

For each component and compound condition, thresholds were measured as the minimum amplitude required for reliable detection (RF vs circle) or discrimination (RF with pedestal amplitude vs RF with pedestal + increment amplitude). As the main aim was to determine how the weighting of each component influenced the thresholds for the compounds, the results are shown as summation plots (Fig. 5). Within each summation plot, the threshold amplitude ($A$) for compound detection/discrimination is expressed by the respective amplitude of each component at the point where the compound was at threshold. That is, the x and y axes give $A·w_1$ and $A·w_2$. This allows one to appreciate how threshold amplitude of each component varied as a function of their contributions (weight) to the compound. The ordinate in all plots shows the higher RF and the abscissa the lower RF component. Each compound condition was tested with five different component weights (100%/0%, 75%/25%, 50%/50%, 25%/75% and 0%/100%). The first percentage corresponds to the lower RF, the second to the higher one. The data point on the x-axis gives baseline thresholds for the lower RF component presented on its own (weight 100%/0%); the data point on the y-axis that for the higher RF (weight 0%/100%).

The left column in Fig. 5 shows the data for detecting shapes against a circle (reference shape with $A = 0$), whereas the right column shows thresholds for discriminating two non-circular shapes (pedestal $A = 0.05$). Different lines in each plot shows data for different phase combinations of the RF components, indicated by different colors (in-phase: red; out-of-phase: blue; intermediate: magenta).

Considering baseline sensitivities to the components first (data points on axes), average thresholds for pure RF patterns are in the same range as previously reported (Bell et al., 2009; Bell & Badcock, 2008; Loffler et al., 2003; Schmidtmann et al., 2012; Schmidtmann & Kingdom, 2017; Wilkinson et al., 1998): slightly lower sensitivities (higher thresholds) for lower RFs than higher RFs (mean threshold across subjects ($\pm$ SEM), RF3: 0.01086 (0.00135) and RF4: 0.00838 (0.00075) compared to RF5: 0.00467 (0.00043), RF7: 0.00474

(0.00092) and RF8: 0.00336 (0.00028)).

Thresholds for discriminating non-circular shapes (right column) are slightly higher (data further away from the origin) than thresholds for detection against a circle (left column). Such an increase in thresholds with increasing reference amplitude has been reported before and found to be small for the amplitudes used here (Bell et al., 2009; Schmidtmann et al., 2012). Thresholds are similar for different phase relationships with the intermediate-phase conditions typically yielding slightly lower thresholds than the in-phase conditions.

Differences between conditions were analysed statistically with a repeated measures ANOVA with phase relationship (in-phase and intermediate), modulation amplitude ($A = 0$; $A = 0.05$), RF combination (RF5/RF3, RF8/RF3, RF7/RF4) and relative weight (0–100%) as factors. The analysis revealed no significant differences between the in-phase and intermediate-phase conditions ($F_{1,16} = 11.74$, $p = .076$), between different reference amplitudes ($F_{1,16} = 3.687$, $p = .195$) or between different RF combinations ($F_{2,16} = 6.381$, $p = .057$). However, a significant main effect was found for the different component weights ($F_{4,16} = 58.06$, $p < .001$). Post-hoc Bonferroni-corrected tests showed that thresholds for the higher frequency component (RF5, RF7, RF8) were significantly lower than for the lower frequency component (RF3, RF4; $p < .05$). Due to the additional out-of-phase condition for combinations between RF3 and RF5, a separate ANOVA was applied with three phase arrangements, five weights and two reference amplitudes as factors. Again, neither phase nor amplitude show significant differences, but weight did: phase ($F_{2,16} = 1.161$, $p = .400$); amplitude ($F_{1,16} = 8.031$, $p = .105$); weight ($F_{4,16} = 65.326$, $p < .001$).

### 3.1. Model simulations

It is clear from the data in Fig. 5 that thresholds are better for the compound conditions than for individual components alone. This rules out a winner-take-all summation, so we are left with PS and AS. To model the data under PS and AS, we used a modified version of the Palamedes Toolbox multi-fit summation function PAL_SDT_Summ_-MultiplePFML_Fit (Prins & Kingdom, 2018). The modification enabled us to set the number of monitored channels Q to be different for the components (Q can be 1 or 2) and the compounds (Q equals 2).

The routine was used to simultaneously fit the four free parameters, gain ($g_A$, $g_B$) and transducer ($\tau_A$, $\tau_B$) as per Eqs. (2a) and (3b) to the five relevant conditions: two components (e.g. RF5: 100%/0%, RF3: 0%/100%) and 3 compounds (e.g. RF5/RF3 with 75%/25%, 50%/50%, 25%/75% weights). Parameters were derived separately for each observer, each phase relationship and each model (PS and AS). Once the parameters are set, percent correct responses for any stimulus level can be simulated, psychometric functions (Logistic) modeled and predicted thresholds extracted. Fitting all five conditions simultaneously provides a better fit than the alternative of first fitting the component data, then using these fits to test how well the AS and PS models fit the compound conditions. The simultaneous fitting method uses all the data, both from component and compound, to test and compare the AS and PS models (Kingdom and Prins, 2016). Typically, the AS model predicts a more linear dependency of thresholds on the amplitudes of the two components when presented within summation plots, whereas the PS model favours a convex curved relationship. As model fits were applied simultaneously to all five conditions in each graph, neither model would be expected to perfectly match the component conditions. If the free parameters ($g_A$, $g_B$, $\tau_A$, $\tau_B$) were derived exclusively from the two component conditions, predictions from both models would be anchored at the component data points, but the overall fit to all conditions would be poorer. All model fits can be found here: http://www.gunnar-schmidtmann.com/stimuli-software/#CompoundRF.

Both models, AS and PS, generally provide a good approximation to the data. The PS and AS model fits were compared by calculating the difference in the Akaike Information Criterion (AIC) between the models (Akaike, 1974; Kingdom and Prins, 2016), such that negative
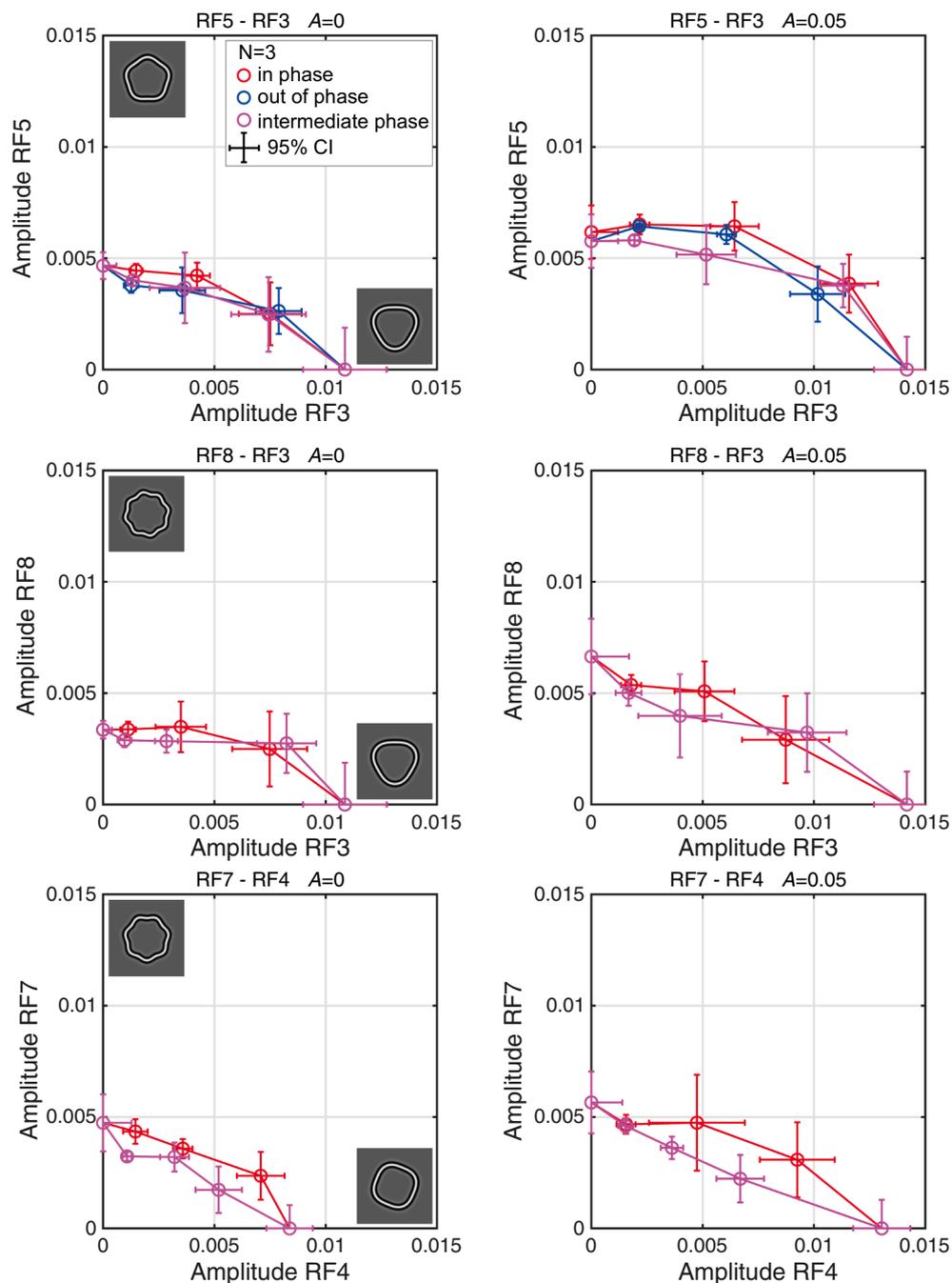
**Fig. 5.** Summation plots showing the threshold amplitudes for detection (left column) and discrimination (right) of compound shapes made up of two RF components. Thresholds for the compound are expressed as the respective amplitudes of the two components (x-axis: lower RF frequency; y-axis: higher frequency) when the compound is at threshold (i.e. $A \cdot w_1$ or $A \cdot w_2$). Thresholds were measured for combinations of RF5/RF3 (top), RF8/RF3 (middle) and RF7/RF4 (bottom). Data for different phase conditions are presented in each plot: in-phase (red), out-of-phase (blue; only for RF3/RF5 combination) and intermediate phase (magenta). The icons show examples of the two components at supra-threshold amplitudes. The error bars represent 95% confidence interval. Individual results can be downloaded here: http://www.gunnar-schmidtmann.com/stimuli-software/#CompoundRF. (For interpretation of the references to color in this figure legend, the reader is referred to the web version of this article.)

values favor AS and positive values favor PS. The complete model comparisons for each observer and all conditions, including the estimated gains $g_A$, $g_B$ and transducer exponents $\tau_A$, $\tau_B$ for each model, AIC and ΔAIC are summarized in tables provided in the Supplementary material. The conditions where PS showed a better model fit are indicated by positive ΔAIC values, whereas the conditions where AS is the preferred model are indicated by negative ΔAIC values. The average transducer exponents for the AS model are: Fixed Attention Window $\tau_A = 1.17$ ( ± SD = 0.25) and $\tau_B = 1.04$ ( ± SD = 0.27); Matched Attention Window: $\tau_A = 1.00$ ( ± SD = 0.26) and $\tau_B = 1.01$ ( ± SD = 0.28). The average transducer exponents for the PS model are: Fixed Attention Window $\tau_A = 1.01$ ( ± SD = 0.26) and $\tau_B = 0.91$ ( ± SD = 0.23); Matched Attention Window: $\tau_A = 1.03$ ( ± SD = 0.29) and $\tau_B = 0.95$ ( ± SD = 0.25). This indicates an approximately linear transducer and explains the approximately straight lines in summation plots. The average transducer exponent for the Single Channel AS

model is $\tau = 0.89$ ( ± SD = 0.12). . Comparing the AS and PS summation models, AS provides better model fits in 33 out of 42 conditions (78%) for the Fixed Attention Window scenario and in 32 out of 42 conditions (76%) for the Matched Attention Window scenario. Comparing the two Attention scenarios, we found that the Fixed Attention Window scenario gave better overall fits (smaller AIC values) than the Matched Attention Window scenario in 88% of the cases for PS and 83% for AS. This suggests that observers were monitoring more than one channel in the component conditions and, by extension, some irrelevant channels, which contribute noise but no signal to the decision.

However, the differences in AIC values between the PS and AS models are relatively small. According to Burnham and Anderson (2004), the preferred model can be determined by calculating the difference between the AIC scores of the *i-th* model ($AIC_i$) and the model with the lowest AIC score ($AIC_{min}$) obtained from the set of models examined, so that
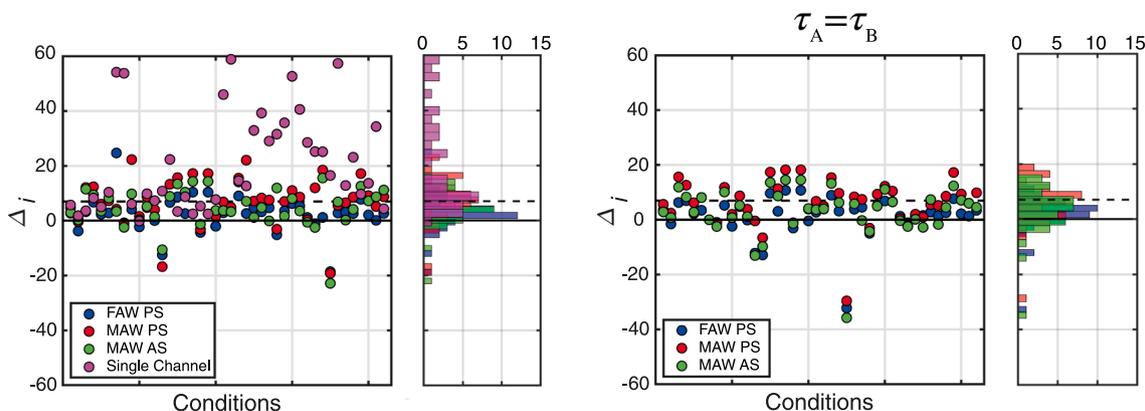
**Fig. 6.** The figure shows the model results across observers. $\Delta_i$ (see Model Simulations section) was calculated for each condition for PS FAW (blue), PS MAW (red), AS MAW (green) and the Single Channel AS model (pink). $\Delta_i$ for the models with the fixed transducer exponents ($\tau_A = \tau_B$) are shown in the right plot. Each graph also contains a marginal histogram of $\Delta_i$ with the color corresponding to the model. Models with $\Delta_i > 7$ can be rejected (Burnham & Anderson, 2004). This threshold is indicated by the dashed black line in each graph. According to this criterion, 14% of the PS FAW fits, 57% of the PS MAW fits, 43% of the AS MAW fits and 74% of the Single Channel fits can be rejected. (For interpretation of the references to color in this figure legend, the reader is referred to the web version of this article.)

$$\Delta_i = AIC_i - AIC_{min} \qquad\qquad\qquad (5)$$

The model with the smallest AIC values is the additive summation fixed-attention window model (AS FAW).

Fig. 6 (left) shows the results for this analysis across observers and shows $\Delta_i$ calculated for each condition for PS FAW (blue), PS MAW (red), AS MAW (green) and the Single Channel AS model (pink). $\Delta_i$ for the models with the fixed transducer exponents are shown in the right plot. The graph also contains a marginal histogram of $\Delta_i$ with the corresponding colors. Models with $\Delta_i > 7$ can be rejected (Burnham & Anderson, 2004). This threshold is indicated by the dashed black line in each graph. According to this criterion, 14% of the PS FAW fits, 57% of the PS MAW fits, 43% of the AS MAW fits and 74% of the Single Channel AS models can be rejected.

In the above analysis, we allowed the transducer exponents for the two components $\tau_A$, $\tau_B$, to be different. However, one could argue that they should be constrained to be equal. To evaluate the effect of such a constraint, we also modeled the data with fixed transducer exponents for both, the Fixed and Matched Attention Window Scenario for all subjects. The results are shown on the right hand side in Fig. 6 ($\tau_A = \tau_B$) and the model parameters are summarized in Table A2-C2. As before, the Fixed Attention Window scenario gives better overall fits (smaller AIC values) than the Matched Attention Window scenario. Note, that for one condition (GS: RF3-8, in phase, $A = 0$) the model simulations did not converge.

Assuming equal transducers, AS provides a better prediction than PS in 30 out of 41 (73%) conditions for the Fixed Attention Window and 38 out of 41 (93%) for the Matched Attention Window scenario. The average transducer exponents for the AS model are: Fixed Attention Window $\tau = 1.05$ ($\pm$ SD = 0.15) ($\tau_A = \tau_B$); Matched Attention Window: $\tau = 0.98$ ($\pm$ SD = 0.15). The average transducer exponents for the PS model are: Fixed Attention Window $\tau = 0.91$ ($\pm$ SD = 0.13) ($\tau_A = \tau_B$); Matched Attention Window: $\tau = 0.94$ ($\pm$ SD = 0.15). This also indicates an approximately linear transducer in all conditions. The comparison of the two Attention scenarios revealed that, assuming equal transducers, the Fixed Attention Window scenario gave better overall fits (smaller AIC values) than the Matched Attention Window scenario in 90% of the cases for PS and 73% for AS. The comparison between the AIC values of the preferred model (model with the smallest AIC values is the additive summation fixed-attention window model) for the fixed transducer condition ($\tau_A = \tau_B$) is presented in Fig. 6 (right). Results show that 12% of the PS Fixed Attention Window models, 45% of the PS Matched Attention Window models and 29% of the AS Matched Attention Window models can be rejected.

Fig. 7 shows $\Delta_i$ values for the PS FAW, PS MAW, AS MAW and the

corresponding models for the fixed transducer exponents ($\tau_A = \tau_B$) condition for each observer (left). A normal distribution was fit to the data (for each observer, averaged across conditions) which is presented in the marginal histogram (right). This analysis illustrates that the model predictions were similar for each observer, despite differences in absolute thresholds (Fig. 5).

In summary, the model simulations favour additive summation of information in excess of the predictions by PS, with observers adopting a strategy of always monitoring the channels of both RF components even if this is strategy is suboptimal as in the case of components presented alone.

## 4. Discussion

The aim of this study was to investigate how the signals from two RF components are combined when observers are asked to discriminate between compound shapes made up of two components with various relative weights.

All in all, we tested nine possible summation scenarios: winner-take-all, PS and AS (Fig. 2) Matched and Fixed Attention Window scenarios with and without fixed transducer exponents and a Single Channel model. The data clearly rejected the winner-take-all scenario. Given that the vast majority of fits (74%) with the Single Channel model were rejected, we conclude that this model does not provide a reasonable account of the data. Although both, PS and AS provide a satisfactory fit to the data, goodness-of-fit comparisons of the two models showed that AS gave the better fit in the large majority of conditions (see Fig. 6). The superiority of AS over PS was found irrespective of whether one assumed that the observer always monitored both RF component-sensitive channels (Fixed Attention Window), or only those channels for which an RF component was present (Matched Attention Window). These results support the idea that compound RF detection is mediated by putative separate channels whose information is subsequently combined into a single channel before a decision rule is applied, as illustrated in Fig. 2C. This combination could be local, i.e. within spatially limited parts of the shape, or global. This conclusion is in line with previous investigations (Dickinson et al., 2013, 2018).

With regards to observer ability to attend to one, or both of the two putative component (RF) channels, our results favour the latter, Fixed Attention Window scenario, which fitted the data better than the Matched Attention Window scenario. This suggests that observers always monitored both channels, irrespective of whether the stimulus was a component or compound. Remember that sensitivity to the components alone would be predicted to be better than we observed if
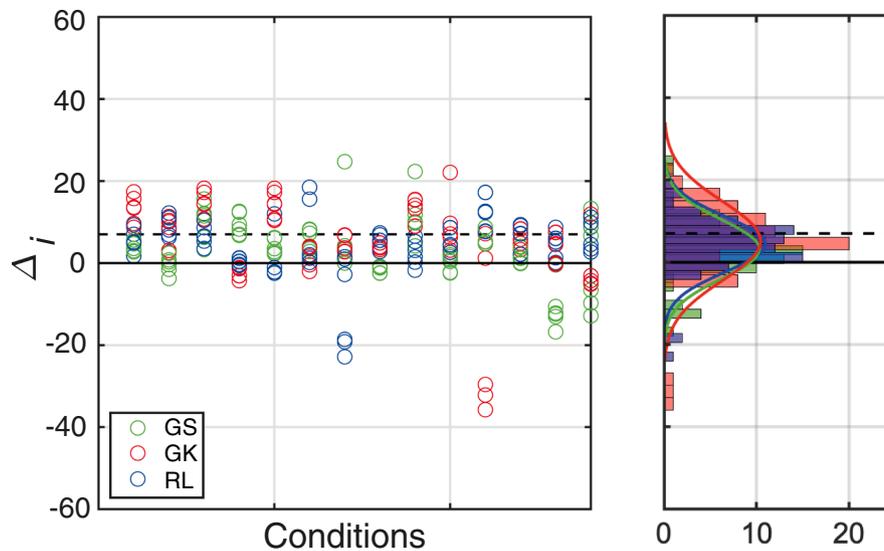
**Fig. 7.** The graph shows $\Delta_i$ values for the PS FAW, PS MAW, AS MAW and the corresponding models for the fixed transducer exponents ($\tau_A = \tau_B$) condition for each observer (left). Normal distributions were fit to the data and are presented in the marginal histogram (right).

observers ignored the channel not containing a signal. The obligatory additive summation of task-irrelevant information with AS under the Fixed Attention Window scenario means that performance is limited by the noise summed from two channels into one mechanism, as indicated in Fig. 2C. Note that our results do not provide evidence that observers have access to the outputs from individual RF/component channels. This may have been a consequence of the particular experimental set-up. It would be a matter for future research to determine if obligatory pooling of information from multiple channels into one mechanism is the general rule with compound RF detection or if observers can select other strategies under other conditions.

### 4.1. Relation to models of RF detection

How do our results bear upon existing ideas about how RF patterns are detected? When quantifying the sensitivity for single RF components, various previous studies have suggested a highly efficient signal integration across the circumference of the contour shape (global processing) (e.g. Bell & Badcock, 2008; Bell, Badcock, Wilson, & Wilkinson, 2007; Bell, Wilkinson, Wilson, Loffler, & Badcock, 2009; Dickinson, McGinty, Webster, & Badcock, 2012; Dickinson et al., 2013; Hess, Achtman, & Wang, 2001; Hess, Wang, & Dakin, 1999; Jeffrey, Wang, & Birch, 2002; Loffler, Wilson, & Wilkinson, 2003; Tan, Dickinson, & Badcock, 2013). Thresholds for discriminating circles from RF component shapes are in the hyperacuity range, which has been linked to efficient, non-linear, global pooling of contour information (Hess et al., 1999; Jeffrey et al., 2002, Loffler et al., 2003; Schmidtmann et al., 2012; Schmidtmann, Gordon, Bennett, & Loffler, 2013). More recent psychophysical evidence and modelling suggests that such global pooling might not be necessary and that models based on the detection of local curvature might be sufficient (Mullen et al., 2011; Baldwin, Schmidtmann, Kingdom & Hess, 2016; Schmidtmann & Kingdom, 2017). It is important to bear in mind that our evidence for AS between RF components is not synonymous with global summation, where the information from all parts of the RF pattern are summed within a single mechanism at detection threshold. Our study does not address the issue of whether RF patterns are detected locally or globally, although our results do say something about the issue. AS between the components of a compound RF stimulus within a local region of the stimulus is compatible with both PS and AS of local RF regions across the whole stimulus (Baldwin et al., 2016, but see Green, Dickinson, & Badcock,

2017, 2018a, 2018b).

### 4.2. Curvature

Schmidtmann and Kingdom (2017) demonstrated that a model based on curvature maxima and minima can account for RF and non-RF pattern detection. Fig. 8 shows the dependence of curvature (calculated according to method described in Schmidtmann & Kingdom, 2017) on the phase relationship of a compound consisting of a weighted combination of an RF3 and an RF5 pattern (for a reference of $A = 0.05$) in an out-of-phase (Fig. 8A) and intermediate phase arrangement (Fig. 8B).

The formal definition of curvature is the rate of change of tangent orientation and was calculated according to a method also employed in previous studies (e.g. Schmidtmann & Kingdom, 2017). For a polar function $r(\theta)$, the local curvature $\kappa_{RF}(\theta)$ is defined as

$$\kappa_{RF}(\theta) = \frac{r(\theta)^2 + 2r'(\theta)^2 - r(\theta)r''(\theta)}{(r(\theta)^2 + r'(\theta)^2)^{3/2}} \tag{7}$$

where $r'(\theta)$ and $r''(\theta)$ refer to the first and second derivative of Eq. (1).

As can be seen, the positions of local curvature values, including maxima and minima, depend on relative phase. However, the values of the maximum (Max) and minimum (Min) curvatures across the entire circumference (shown by the red and green markers) and hence also Max-Min curvatures, vary rather little across relative phase. Given that the data show little or no variation in thresholds across relative phase, we cannot rule out the possibility that one or other of Max, Min or Max-Min curvature mediates thresholds in compound RF patterns as suggested by Schmidtmann & Kingdom (2017). Indeed, our finding that AS rather than PS between the two RF components is the better model of compound detection does not necessarily imply an initial stage in which the RF components are separately encoded prior to their combination, even though that is how the AS model is framed. The AS model may be the computational equivalent of a low-level feature model of RF detection and discrimination, such as one based on points of Max or Max-Min curvature. Future data and modeling is required to determine whether the results of this study can also be explained by channels sensitive to these curvature dimensions.

### 4.3. Symmetry

Finally, our results have implications for the role of symmetry in
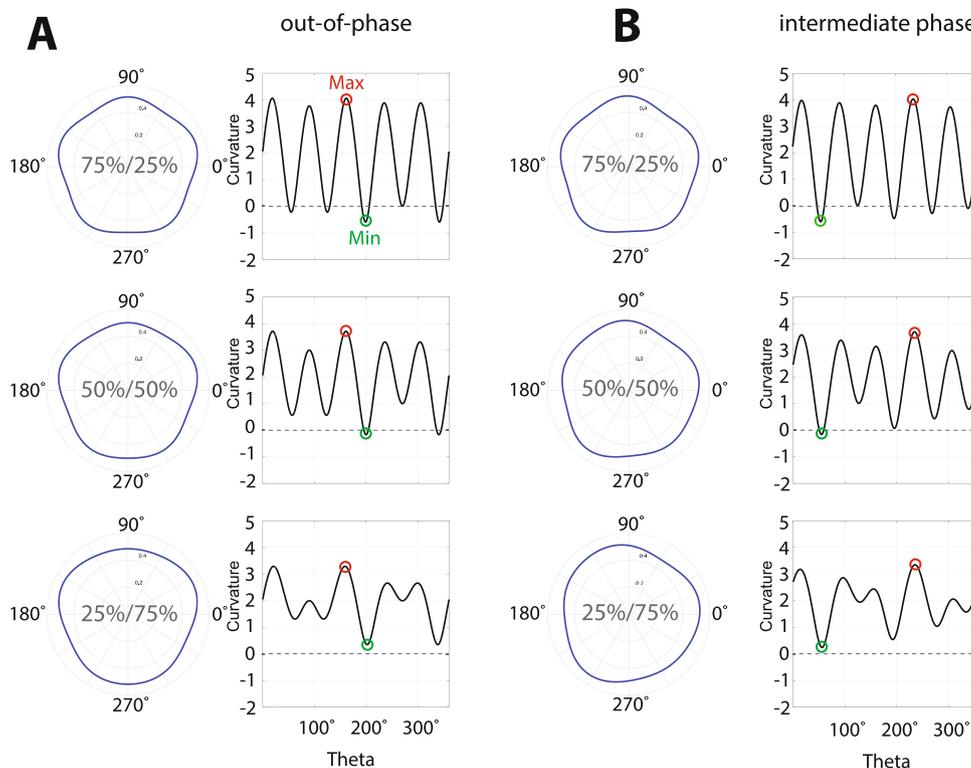
**Fig. 8.** Dependence of curvature on the phase relationship between the two RF components that make up the shape compound. The figure shows compound shapes created by weighted combinations of an RF3 and an RF5 pattern ($A = 0.05$) with different phase arrangements; (A) out-of-phase and (B) intermediate phase. The polar graphs illustrate the shape of the resulting pattern and the adjacent graphs the corresponding curvature profile. Max refers to the maximum and Min to the minimum curvature.

shape discrimination. Pure RF components, and compound RFs with in-phase and out-of-phase relationships, are bilateral, mirror-symmetrical shapes. For instance, a pure RF3 has three, and a pure RF5 five axes of symmetry. Compound RF shapes that are either in-phase or out-of-phase have only one axis of symmetry. In contrast, compound RF shapes at intermediate phase arrangements are asymmetric as can be seen in Fig. 8B. Symmetry in general, and bilateral symmetry in particular, have been shown to play a special role in human perception and have been the subject of a vast number of investigations (see Treder, 2010 for review). If humans are especially sensitive to symmetry, then one might expect lower discrimination thresholds for symmetric compound patterns compared to those that lack symmetry. This was not what we found. One possible explanation is that the orientation of the RF patterns was randomly varied between trials. This was used in order to avoid subjects from predicting the exact position of specific parts of the contour (e.g. curvature maximum) or to focus on a particular part (cycle) of the shape. Previous studies on symmetry processing have shown that performance is best for vertical axes of symmetry, followed by horizontal and oblique ones (Barlow & Reeves, 1979; Wenderoth, 1994). The change in orientation of the symmetry axes in our experiments might have, to some extent, counterbalanced the contribution of a symmetry effect. In any case, we did not find any evidence in favour of symmetry being a beneficial feature in these experiments of shape discrimination.

## Acknowledgments

## Appendix A. Supplementary data

Supplementary data to this article can be found online at https://doi.org/10.1016/j.visres.2019.05.002.

## References

Akaike, H. (1974). A new look at the statistical model identification. *IEEE Xplore: IEEE Transactions on Automatic Control, 19*(6), 716–723.

Baldwin, A. S., Schmidtmann, G., Kingdom, F. A. A., & Hess, R. F. (2016). Rejecting probability summation for RF patterns, not so Quick!. *Vision Research, 122,* 124–134.

Barlow, H., & Reeves, B. (1979). The versatility and absolute efficiency of detecting mirror symmetry in random dot displays. *Vision Research, 19*(7), 783–793.

Bell, J., & Badcock, D. (2009). Narrow-band radial frequency shape channels revealed by sub-threshold summation. *Vision Research, 49*(8), 843–850.

Bell, J., & Badcock, D. R. (2008). Luminance and contrast cues are integrated in global shape detection with contours. *Vision Research, 48*(21), 2336–2344.

Bell, J., Badcock, D., Wilson, H., & Wilkinson, F. (2007). Detection of shape in radial frequency contours: independence of local and global form information. *Vision Research, 47*(11), 1518–1522.

Bell, J., Wilkinson, F., Wilson, H. R., Loffler, G., & Badcock, D. R. (2009). Radial frequency adaptation reveals interacting contour shape channels. *Vision Research, 49*(18), 2306–2317.

Burnham, K. P., & Anderson, D. R. (2004). Multimodel inference: Understanding AIC and BIC in model selection. *Sociological Methods and Research, 33*(2), 261–304.

Brainard, D. H. (1997). The psychophysics toolbox. *Spatial Vision, 10*(4), 433–436.

Campbell, F., & Robson, J. (1968). Application of Fourier analysis to the visibility of gratings. *Journal of Physiology, 197*(3), 551–566.

Dickinson, J. E., Bell, J., & Badcock, D. R. (2013). Near their thresholds for detection, shapes are discriminated by the angular separation of their corners. *PLoS One, 8*(5), e66015.

Dickinson, J. E., Haley, K., Bowden, V. K., & Badcock, D. R. (2018). Visual search reveals a critical component to shape. *Journal of Vision, 18*(2), 1–25.

Dickinson, J. E., McGinty, J., Webster, K. E., & Badcock, D. R. (2012). Further evidence that local cues to shape in RF patterns are integrated globally. *Journal of Vision, 12*(12), 16.

Graham, N. (1989). *Visual Pattern Analyzers (Oxford University Press)*. New York: Oxford University Press.

Graham, N., & Nachmias, J. (1971). Detection of grating patterns containing two spatial frequencies: a comparison of single-channel and multiple-channels models. *Vision*

*Research, 11*(3), 251–259.

Green, R. J., Dickinson, J. E., & Badcock, D. R. (2017). Global processing of random-phase radial frequency patterns but not modulated lines. *Journal of Vision, 17*(9), 1–18.

Green, R. J., Dickinson, J. E., & Badcock, D. R. (2018a). Integration of shape information occurs around closed contours but not across them. *Journal of Vision, 18*(5), 1–6.

Green, R. J., Dickinson, J. E., & Badcock, D. R. (2018b). Convergent evidence for global processing of shape. *Journal of Vision, 18*(7), 1–15.

Green, D. M., & Swets, J. A. (1988). *Signal detection theory and psychophysics.* Los Altos, California: Peninsula Publishing.

Hess, R. F., Achtman, R. L., & Wang, Y. (2001). Detection of contrast-defined shape. *Journal of the Optical Society of America A: Optics, Image Science, and Vision, 18*(9), 2220–2227.

Hess, R. F., Wang, Y., & Dakin, S. C. (1999). Are judgements of circularity local or global? *Vision Research, 39*(26), 4354–4360.

Jeffrey, B., Wang, Y., & Birch, E. (2002). Circular contour frequency in shape discrimination. *Vision Research, 42*(25), 2773–2779.

King-Smith, P. E., & Kulikowski, J. J. (1975). The detection of gratings by independent activation of line detectors. *The Journal of Physiology, 247*(2), 237–271.

Kingdom, F. A. A., & Prins, N. (2016). *Psychophysics: A practical introduction* (2nd). Academic Press, an imprint of Elsevier.

Kingdom, F. A. A., Baldwin, A. S., & Schmidtmann, G. (2015). Modeling probability and additive summation for detection across multiple mechanisms under the assumptions of signal detection theory. *Journal of Vision, 15*(5), 1–16.

Kulikowski, J. J., & King-Smith, P. E. (1973). Spatial arrangement of line, edge and grating detectors revealed by subthreshold summation. *Vision Research, 13*(8), 1455–1478.

Laming, D. (2013). Probability summation-a critique. *Journal of the Optical Society of America A, 30*(3), 300–315.

Legge, G. E., & Foley, J. M. (1980). Contrast masking in human vision. *Journal of the Optical Society of America, 70*, 1458–1471.

Loffler, G. (2008). Perception of contours and shapes: low and intermediate stage mechanisms. *Vision Research, 48*(20), 2106–2127.

Loffler, G. (2015). Probing intermediate stages of shape processing. *Journal of Vision, 15*(7), 1–19.

Loffler, G., Wilson, H. R., & Wilkinson, F. (2003). Local and global contributions to shape discrimination. *Vision Research, 43*(5), 519–530.

Macmillan, N. A., & Creelman, C. D. (2005). Detection theory: A user's guide. New York.

Meese, T. S., & Baker, D. H. (2011). Contrast summation across eyes and space is revealed along the entire dipper function by a "Swiss cheese" stimulus. *Journal of Vision, 11*(1), 1–23.

Meese, T. S., & Summers, R. J. (2012). Theory and data for area summation of contrast with and without uncertainty: Evidence for a noisy energy model. *Journal of Vision, 12*(11), 1–28.

Mullen, K., Beaudot, W., & Ivanov, I. V. (2011). Evidence that global processing does not limit thresholds for RF shape discrimination. *Journal of Vision, 11*(3), 1–21.

Nachmias, J. (1981). On the psychometric function for contrast detection. *Vision Research, 21*, 215–223.

Poirier, F. J. A. M., & Wilson, H. R. (2006). A biologically plausible model of human radial frequency perception. *Vision Research, 46*(15), 2443–2455.

Prins, N., & Kingdom, F. A. A. (2018). Applying the model-comparison approach to test specific research hypotheses in psychophysical research using the Palamedes toolbox. *Frontiers in Psychology, 9*, 1250.

Sachs, M., Nachmias, J., & Robson, J. (1971). Spatial-frequency channels in human vision. *Journal of the Optical Society of America, 61*(9), 1176–1186.

Schmidtmann, G., & Fruend, I. (2019). Radial frequency patterns describe a small and perceptually distinct subset of all possible planar shapes. *Vision Research, 154*, 122–130.

Schmidtmann, G., Gordon, G. E., Bennett, D. M., & Loffler, G. (2013). Detecting shapes in noise: tuning characteristics of global shape mechanisms. *Frontiers in Computational Neuroscience, 7*(37), 1–14.

Schmidtmann, G., Jennings, B. J., Bell, J., & Kingdom, F. A. A. (2015). Probability, not linear summation, mediates the detection of concentric orientation-defined textures. *Journal of Vision, 15*(16) 6. 1–19.

Schmidtmann, G., Kennedy, G. J., Orbach, H. S., & Loffler, G. (2012). Non-linear global pooling in the discrimination of circular and non-circular shapes. *Vision Research, 62*, 44–56.

Schmidtmann, G., & Kingdom, F. A. A. (2017). Nothing more than a pair of curvatures: A common mechanism for the detection of both radial and non-radial frequency patterns. *Vision Research, 134*(2017), 18–25.

Tan, K. W. S., Dickinson, J. E., & Badcock, D. R. (2013). Detecting shape change: Characterizing the interaction between texture-defined and contour-defined borders. *Journal of Vision, 13*(14), 1–16.

Treder, M. S. (2010). Behind the looking-glass: A review on human symmetry perception. *Symmetry, 2*(3), 1510–1543.

Tyler, C. W., & Chen, C.-C. (2000). Signal detection theory in the 2AFC paradigm: Attention, channel uncertainty and probability summation. *Vision Research, 40*, 3121–3144.

Wenderoth, P. (1994). The salience of vertical symmetry. *Perception, 23*, 221–236.

Wilkinson, F., Wilson, H. R., & Habak, C. (1998). Detection and recognition of radial frequency patterns. *Vision Research, 38*(22), 3555–3568.